A flexible strain-responsive sensor fabricated from a biocompatible electronic ink via an additive-manufacturing process

James Britton [a,*], Katarzyna Krukiewicz [a,b,*], Malu Chandran [a], Jorge Fernandez [c], Anup Poudel [a], Jose-Ramon Sarasua [d], Una FitzGerald [a], Manus J.P. Biggs [a,*]

[a] Centre for Research in Medical Devices, National University of Ireland, Galway, Newcastle Road, H91 W2TY Galway, Ireland
[b] Department of Physical Chemistry and Technology of Polymers, Silesian University of Technology, M.Strzody 9, 44-100 Gliwice, Poland
[c] Polimerbio, S.L, Paseo Mikeletegi 83, 20009 Donostia-San Sebastian, Spain
[d] Department of Mining-Metallurgy Engineering and Materials Science, POLYMAT, University of the Basque Country (UPV/EHU), School of Engineering, Alameda de Urquijo s/n, 48013 Bilbao, Spain

HIGHLIGHTS

- We developed strain-responsive biosensors from biocompatible conductive polymer inks.
- We developed a scalable additive manufacturing process to print custom sensor designs.
- The cytocompatibility of this ink was assessed *in-vitro* with a mixed neural cells.
- The biosensing capabilities were evaluated under simulated physiological conditions.

GRAPHICAL ABSTRACT
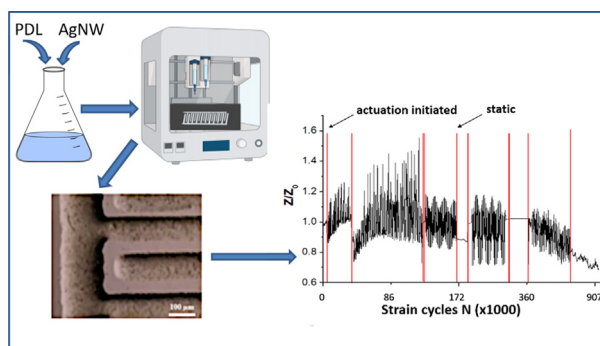
ABSTRACT

Biosensor technologies are of great interest for applications in wearable electronics, soft robotics and implantable biomedical devices. To accelerate the adoption of electronics for chronic recording of physiological parameters in health and disease, there is a demand for biocompatible, conductive & flexible materials that can integrate with various tissues while remaining biologically inert. Conventional techniques used to fabricate biosensors, such as mask lithography and laser cutting, lack the versatility to produce easily customisable, micro-fabricated biosensors in an efficient, cost-effective manner. In this paper, we describe the development and characterisation of an electronic ink made from an environmentally sustainable copolymer - ω-*pentadecalactone-co-ε-decalactone*, (PDL) incorporating silver nanowires (AgNW), which are known for their antimicrobial and conductive properties. The composites were shown to possess a low percolation threshold (1% w/w of AgNW to PDL), achieve a low electrical resistance (320 ± 9 Ω/sq) and a high electrical capacitance (2.06 ± 0.06 μF/cm^2). PDL nanocomposites were biocompatible, demonstrated *in vitro* through the promotion of neural adhesion and prevention of astrocyte activation. An optimised ink formulation was subsequently used to fabricate strain-responsive biosensors with high spatial resolution (sub – 100 μm) using a direct write additive manufacturing process. Using a customized *in vitro* set-up, the sensitivity of these biosensors to biologically-relevant strains was assessed under simulated physiological conditions for 21 days. Critically, these 3D printed biosensors

∗ Corresponding authors at: Centre for Research in Medical Devices, National University of Ireland, Galway, Newcastle Road, H91 W2TY Galway, Ireland.

have applications in chronic prophylactic monitoring of pressure changes within the body and related pathologies.

1. Introduction

Currently, clinical practice is undergoing a transition to an era of continuous precision monitoring of physiological parameters using wearable or implantable electronic sensors, reducing healthcare costs and improving patient care [1]. The clinical translation of implantable sensor devices that facilitate continuous data acquisition is hampered however, by issues stemming from invasive surgery, immune rejection, and the risk of infection/trauma during device retrieval or removal. To overcome this problem, biosensors must be fabricated from biocompatible, highly flexible materials using a manufacturing process that is both financially competitive and scalable to industrial production technologies [2].

Biosensors that can provide precise, real-time measurements of physiological parameters have huge potential in both personalised medicine and biomedical meta-analysis. For example, the capacity to measure changes in physiological pressure and temperature can provide an early indicator of disease progression and promote timely therapeutic intervention. Recent work in this field has led to the development of implantable strain and pressure sensors that can be used to remotely monitor conditions such as coronary heart disease and intracranial hypertension [3]. Meng et al. developed an effective method to fabricate highly sensitive and flexible wearable strain sensors [4]. Using a layer-by-layer method the formation of a polyurethane/graphene composite film, with outstanding electrical conductivity (1430 ± 50 S/cm) and high strain sensitivity (gauge factor up to 150) was demonstrated. These composites were subsequently fabricated into sensors which facilitated the accurate monitoring of body movements. Similarly, Pang et al. reported the development of a flexible and highly sensitive strain-gauge sensor, composed of high aspect ratio platinum-coated polyurethane-based nanofibers supported by a polydimethylsiloxane substrate, allowing for the detection of pressure, shear and torsion [5]. These sensors exhibited high repeatability and reproducibility and were able to monitor multiple intravital signals.

Critically, accurate intracranial pressure monitoring is vital for the management of numerous neurological disorders, including traumatic brain injury or stroke induced swelling [6]. A recent key study by Yang et al. described a bioresorbable intracranial pressure monitoring platform composed of poly(lactic-co-glycolic acid) and monocrystalline silicon sheets as flexible encapsulation layers on a magnesium substrate. Although the sensor was designed to be resorbable, its architecture allowed stable operation for at least 3 weeks, demonstrating a similar performance level to a non-resorbable and clinically available intercranial pressure sensors [7]. In a similar study, we previously described the physicomechanical, electrochemical and active pressure sensing behaviour of an electrically conductive poly(glycerol sebacate urethane) composite, reinforced with poly(3,4-ethylenedioxythiophene) polystyrene sulfonate functionalized carbon nanotubes [8]. By experimentally determining the percolation threshold of this composite, it was possible to obtain a flexible, conducting and durable pressure sensor, suitable for soft tissue engineering and bioelectronic applications.

In recent years, there has been an increased interest in using polymers from sustainable sources in next-generation electronics, and medical implant [9,10]. Poly(ω-pentadecalactone), is an aliphatic polyester exhibiting advantageous tensile strength and biocompatibility, making it applicable to biomedical applications and as a shape memory polymer [11]. Poly(ε-decalactone), is a pliable, biocompatible polymer that can be produced in an environmentally sustainable manner by fungal biotechnology. The copolymers of poly(ω-pentadecalactone) and poly(ε-decalactone) have recently been shown to possess high elongation at break values and low stiffness (secant modulus of 7–156 MPa), together with good mechanical stability, making them ideal for strain sensor applications [11].

Additive manufacturing of implantable devices has progressed rapidly in the last decade [12,13].Today, 3D printing of polymers and metals has become a standard technique used in biomedical engineering to create product prototypes and functional implants. In particular, extrusion-based printing can be used to produce bioelectronics which are both customisable and scalable. This approach uses motorised or pneumatic forces to extrude thermoplastics such as polylactic acid and acrylonitrile butadiene styrene which are commonly used polymers in additive manufacturing but are prone to post-print fracturing upon the application of mechanical strain. Therefore, current approaches have been focused on the introduction of novel inks that posess high flexibility and tunable viscocity, facilitating the extrusion printing of complex geometries [14]. Critically, conventional thermoplastic polymers can be electromechanically enhanced through the incorporation of particulate fillers [15]. The use of silver nanowires (AgNW) in the development of flexible bioelectronics has recently been explored due to their excellent electrical conductivity, low cytotoxicity and antibacterial properties [14,16]. Furthermore, although it has been reported that AgNWs can be toxic when endocytosed by cells, this toxicity can be diminished by using nanowires with a diameter in the region of 30 nm or by embedding the nanowires in a polymer matrix [17]. Furthermore, the application of AgNWs in the design of pressure sensors has been shown to produce devices exhibiting high sensitivity, a broad detection range, a fast response time, and outstanding stability and durability [18].

Here, we report on the development of a strain-responsive biosensor fabricated from ω-pentadecalactone-co-ε-decalactone/AgNW composite bioink using a scalable and customisable direct material writing proces. Specifically, to demonstrate the potential of this fabrication approach, we produced several prototypical geometric electrode designs on flexible substrates. Developed bioinks were found to be cytocompatible, electrically conducting and facilitated the microfabrication of soft piezoresistive electrodes onto pristine pentadecalactone-co-ε-decalactone films. Resulting biosensor devices were shown to exhibit high sensitivity and durability when exposed to simulated physiological strain conditions.

2. Materials and methods

2.1. Synthesis and characterisation of ω-pentadecalactone-co-ε-decalactone copolymer (PDL)

A copolymer of ω-pentadecalactone and ε-decalactone was synthesised according to a procedure described previously (PDL-DL 30 co-polymer) [19]. In short, a 30/70 mass feed ratio of w-PDL/ ε-DL was subjected to a one-pot-one-step ring-opening polymerisation process, conducted in a flask immersed in an oil-bath purged with nitrogen for 30 min. Triphenyl bismuth was used as a catalyst. After six days of polymerisation, the products were dissolved in chloroform, precipitated in methanol, dried at room

temperature and then heated at 140 °C for 1 hr. The resulting copolymer was characterised using ^{1}H and ^{13}C NMR spectroscopy (Bruker Avance DPX 300, MA, USA), differential scanning calorimetry (Q200 instrument, TA Instruments, Delaware, USA), tensile tests (Zwick/Roell Z2.5 testing machine, Ulm, Germany), gel permeation chromatography (Waters 1515 GPC device, MA, USA), wide-angle X-ray diffraction analysis (Bruker D8 Advance diffractometer, MA, USA) and thermogravimetric analysis (TGA model Q50-0545, TA Instruments, Delaware, USA).

2.2. Fabrication of PDL/AgNW composite

PDL was dissolved in a tetrahydrofuran (THF) solvent to form a 10% w/v solution. Following this, 0.1 ml of a 20 mg/mL silver nanowire solution (average diameter 30 nm, average length 100–200 µm, silver purity ~ 99.5%, dispersed in ethanol) was added to the polymer solution. To find the percolation threshold of AgNW content, PDL/AgNW formulations with different concentrations of AgNW/EtOH in PDL/THF were formulated ranging from 0.02% w/w (1 µl of AgNW/EtOH to 1 ml of PDL/THF) to 2% w/w (100 µl of AgNW/EtOH to 1 ml of PDL/THF). For the optimisation process, glass substrates (25 × 25 × 1.0 mm) were used as the support for the PDL/AgNW formulations. Prior to the deposition of a composite film, glass slides were sputter-coated (Emitech K650XT Sputter Coater, Paris, France) at 25 mA, 1×10^{-3} mbar for 180 s) with a 10 nm layer of Pt and pre-treated with an oxygen plasma process (Zepto LF, Diener Electronics, Ebhausen, Germany) for 10 min. Pristine PDL and PDL/AgNW coatings were deposited by spin coating (Laurell Technologies Spin Coater, PA, USA) 0.1 ml of the PDL/AgNW solution for 20 s at a speed of 3000 rpm.

2.3. Physicochemical characterisation of PDL/AgNW

Electrochemical studies were carried out by means of a PARSTAT 2273 potentiostat in a three-electrode set-up, comprising a glassy carbon rod as an auxiliary electrode, Ag/AgCl as a reference electrode and a working electrode of PDL or PDL/AgNW-coated Pt/-glass slide, as well as a bare Pt/glass slide as a control. The percolation threshold was assessed with respect to the charge storage capacity (CSC) of materials, which was determined by obtaining cyclic voltammetric (CV) curves collected in 0.1 M KCl solution within a potential range from −0.8 to 1.0 V (vs. Ag/AgCl) at 100 mV/s for 5 CV cycles, and calculated according to the formula:

$$CSC = \int_{t_1}^{t_2} I(t)dt$$

where t_1 is the start time of the CV cycle, t_2 is the end time of a CV cycle, and I is the current density.

Electrochemical impedance spectra (EIS) were collected in a 0.1 M KCl solution with frequencies ranging from 0.1 Hz to 100 kHz, an AC amplitude of 40 mV (vs. Ag/AgCl) and a DC potential equal to 0 V (vs. Ag/AgCl). The results were presented in the form of Bode plots. EIS Spectrum Analyzer 1.0 software [20] and the Powell algorithm were used to fit the experimental data to an equivalent circuit model. Capacitance was calculated based on the parameters of a constant phase element (CPE) according to the formula:

$$C = \frac{(P \cdot R)^{1/n}}{R}$$

where C is the capacitance (F), R is the film resistance (Ω), P and n are CPE parameters.

To evaluate the viscoelastic properties of the pristine and composite electronic inks, dynamic rheological testing was performed using an Anton Parr MCR 302 system with a 10 mm parallel plate configuration. A fixed distance of 1 mm at a constant temperature was maintained for each sample analysed. The complex viscosity over a range of strain rates from 0.1 to 100% at a constant frequency of 1 Hz was assessed for all the polymer inks developed. Similarly, to determine the mechanical properties of the solid PDL and nanocomposite substrates after curing (solvent evaporation), 12 mm discs of 1 mm height were cut using a tissue puncher and subjected to rheological testing. The storage modulus of 2w/w AgNW – PDL was of particular interest as this composition provided favorable 3D printing properties. The storage modulus over a range of strain rates from 1 to 100% was assess at a constant frequency of 1 Hz [21].

2.4. In vitro biological characterisation of PDL/AgNW

All experiments were performed in accordance with the European guidelines (2010/63/EU) and were approved by the Health Products Regulatory Authority (AE19125/I179) and the National University of Ireland, Galway (ACREC) research ethics committee. Every effort was made to minimise animal suffering and to reduce the number of animals used.

Primary cultures of a mixed neural population obtained from the ventral mesencephalon (VM) of E14 rat embryos were used as an *in vitro* model to assess the cytocompatibility of the pristine PDL and a PDL/AgNW composite material, according to the protocol described in Refs. [22–24]. In short, the embryos were obtained by laparotomy from time-mated female Sprague-Dawley rats (Charles River Laboratories, MA, USA). VM cells were dissected from embryonic rat brains, dissociated and cultured in a humidified atmosphere (5% CO_2, 37 °C), in Dulbecco's modified Eagle's medium D6421 (Sigma-Aldrich, Dublin, Ireland) supplemented with 1% w/v D-glucose, 1% v/v L-glutamine, 1% v/v penicillin/streptomycin, 10% v/v foetal calf serum (FCS) and 2% v/v B27 (Invitrogen, CA, USA). PDL or PDL/AgNW-coated Pt/glass slides, as well as bare Pt/glass slide controls, were placed in 12-well culture plates, sterilised in 70% ethanol for 2 hrs, washed repeatedly with Hank's balanced salt solution (Sigma, MO, USA), coated with 1% w/v poly-L-lysine (Sigma, MO, USA) rinsed with distilled water and left to dry. A quantity of 50 000 cells/cm² was plated on each film, and then 2 ml of the culture medium was added to each well and changed with fresh media every two days for a period of seven days.

Neurons and astrocytes were visualised through indirect double-immunofluorescent labelling. VM cells were first fixed with 4% paraformaldehyde for 30 min and then washed three times with 1x PBS before permeabilisation with 0.5% Triton X-100 in 1X PBS for 10 min. A 1% Bovine serum albumin (BSA) solution was used to block nonspecific binding sites. VM cells were then incubated with anti-glial fibrillary acidic protein antibody (catalogue no. G3893, Sigma, MO, USA) produced in mouse and anti-β-Tubulin III antibody (catalogue no. T2200, Sigma, MO, USA) produced in rabbit. After washing, samples were incubated in the secondary antibody Alexa Fluor 488 goat anti-mouse IgG/IgA/IgM (H + L) (catalogue no. SAB4600387, Sigma, MO, USA) combined with the secondary antibody Alexa Fluor 594 goat anti-rabbit IgG (H + L) (catalogue no. SAB4600322, Sigma, MO, USA). Samples were washed with PBS, mounted on glass-bottomed dishes (IBIDI, London, England) and counterstained with DAPI Slowfade® Gold Antifade Mountant (catalogue no. S36937, Thermo Fisher Scientific, MA, USA) for nuclear staining

After immunostaining, samples were viewed with the use of an Olympus Fluoview 1000 Confocal Microscope (scan size of 1024 × 1024 at a ratio 1:1 and 60× magnification). Cell density was analysed by counting the number of nuclei corresponding to neurons and astrocytes in an area of 600 µm² in at least 20 random images taken from test and control groups. The same set of

fluorescent images was used to determine the mean area of astrocytes, as carried out with the use of ImageJ (NIH) image analysis software.

2.5. Design and fabrication of stain gauge biosensors using additive manufacturing

In order to design strain gauge biosensors from an AgNW composite bioink, computer-aided design (CAD) software (Autodesk inventor 2017, student edition) was used to design electrode geometries with increasing complexity. Initial designs consisted of simple linear-shaped electrodes, developed to a final 60-interdigitated probe design (Fig. S1). 3D CAD drawings were exported in the standard triangular language (STL) format and sliced using software provided by GeSIM mbH (Radeberg, Germany). BioScaffolder 3.2. 3D models were sliced at a strand-width and height of 150 μm to accommodate the diameter of the extrusion needle and to fabricate biosensors that challenged the upper limits of this additive manufacturing process while adhering to recently defined American Society for Testing and Materials ISO/ASTM 52910:2018(E) additive manufacturing international standards.

Pneumatic pressure propelled extrusion-based 3D printing (Movie S1) was used to deposit thin filaments of the PDL/AgNW composite through a 150 μm nozzle tip (catalogue no. 7018424, Nordson, EFD, RI, USA). 3D print parameters were initially optimised to facilitate the deposition of a continuous filament onto a flexible thermanox print substrate. 3D print parameters of 5 mms^{-1} print velocity, 75 kPa pneumatic pressure at a temperature of 37 °C were optimal for the fabrication of composite biosensors. The THF solvent evaporated quickly after deposition within a biological flow hood.

2.6. Morphological characterisation of 3D printed biosensors

The macrostructure of 3D printed biosensors was evaluated using light microscopy at 10X and 20X magnification (EVOS XL Core imaging system). The integrity of 3D printed filaments and the maintenance of silver nanowire dispersion within the composite ink were evaluated using a Digital microscope (DSX510, Olympus, Tokyo, Japan). Image J analysis software was used to quantify filament diameter and nanofiber length. Scanning Electron Microscopy (SEM) images were collected with a Scanning Electron Microscope (Hitachi S-4700, Tokyo, Japan) operating at 15 kV acceleration voltage.

2.7. In vitro analysis of strain response of biosensors

Biosensors were characterised *in vitro* using a CellScale MCT6 bioreactor apparatus (Fig. S2). Changes in electrochemical resistance were measured with a Potentiostat (Princeton Applied Research, model 2273) and Power suite software. 3D printed AgNW/PDL biosensors were first electroded by bonding wires using conductive silver epoxy. Initially, three biosensors were clamped to the struts of the actuation device using metallic grips. Samples were exposed to normal physiological conditions by suspending the biosensors in a bath of Phosphate Buffered Saline (PBS), and the temperature maintained at 37 °C using a temperature probe controlled hot-plate. A 60 interdigitated electrode strain sensor was subjected to linear actuation at a strain rate of 5% at a frequency of 0.5 Hz and a loading capacity of 200 N [25]. The potentiometric readout was obtained using an AC sinusoidal input of 1 V at a single frequency of 1 kHz. Impedance readouts were acquired daily for 21 days in order to assess the stability of the biosensor device. This experiment facilitated the simultaneous evaluation of the biosensors resilience to degradation under physiological conditions, which would be evident from changes in biosensor recording stability.

2.8. Statistical analysis

For all biological experiments, both the test and control groups included three biological replicates. The cell density and mean astrocyte area was analysed based on at least 20 random images taken from test and control groups. The results were expressed as the mean of the values ± standard error of the mean, and the statistical significance was determined using a Student *t*-test (p < 0.05). Mechanical analysis of PDL and PDL/AgNW samples were carried out on three replicate devices. The viscoelastic properties of each sample group are expressed as the mean ± SD over a range of strain rates. For biosensor sensitivity measurements, the relative change in impedance was determined from three biosensors and expressed as mean strain gauge factor change ± SD, where SFG was calculated from the change in impedance / average impedance measured during cyclic strain loading.

3. Results and discussion

3.1. Determination of the percolation threshold

To determine the minimum amount of AgNWs that provide conductive behaviour to a PDL/AgNW composite material, cyclic voltametric (CV) curves of composites with different PDL-to-AgNWs ratio were collected (Fig. 1A), and the corresponding charge storage capacities were calculated (CSC, Fig. 1B). Since PDL is not an intrinsically conducting polymer and does not undergo reversible oxidation/reduction processes, its corresponding CV curve was flat. The addition of AgNWs (below 0.2% w/w) did not have any significant effect on the shape of CV curve. The addition of 0.4% w/w content however gave rise to redox peaks associated with the reversible reduction (−0.13 V vs. Ag/AgCl) and oxidation (0.25 V vs. Ag/AgCl) of silver in the CV curve. For this formulation an increase in the area below the graph, associated with a corresponding increase in the capacitance of the composite material was also noted. With a further increase in AgNW content, an increase in the redox current density as well as capacitance was observed and a minimum content of 2% w/w was required in order for the electrochemical properties to stabilise. The percolation behaviour of the PDL/AgNW composite was observable from the changes in the CSC, which were calculated by integrating corresponding CV curves with respect to time. CSC is the parameter of crucial importance in biosensing applications, since it determines if the material is able to store relatively large charges before reaching an over-potential where irreversible faradaic reactions occur [26]. Increasing the AgNWs content to more than 0.4% w/w resulted in a dramatic increase in the CSC, reaching a plateau at 1% w/w (Fig. 1).

From this data, we have demonstrated that silver nanowires can be used to tailor the conductivity of PDL and that the percolation threshold can be achieved at a concentration of 0.4% w/w AgNW to PDL. Although silver nanoparticles have been explored previously as conducting fillers for various non-conducting polymers, the percolation threshold was relatively high, circa 15 vol% [27,28]. AgNWs, due to their large aspect ratio (~5000), can reach the percolation threshold at a lower content. For example, Wang et al. [29] showed that when the filler content of AgNWs in a polyurethane composite increased from 0 to 3 wt%, its relative dielectric permittivity increased from 5.4 to 45.3. Similarly, Langley et al.[30]studied the ability of AgNWs to form a robust percolation path and determined the optimal AgNWs surface density needed to reach low electrical resistance at ~100 mg/m². In our study, the
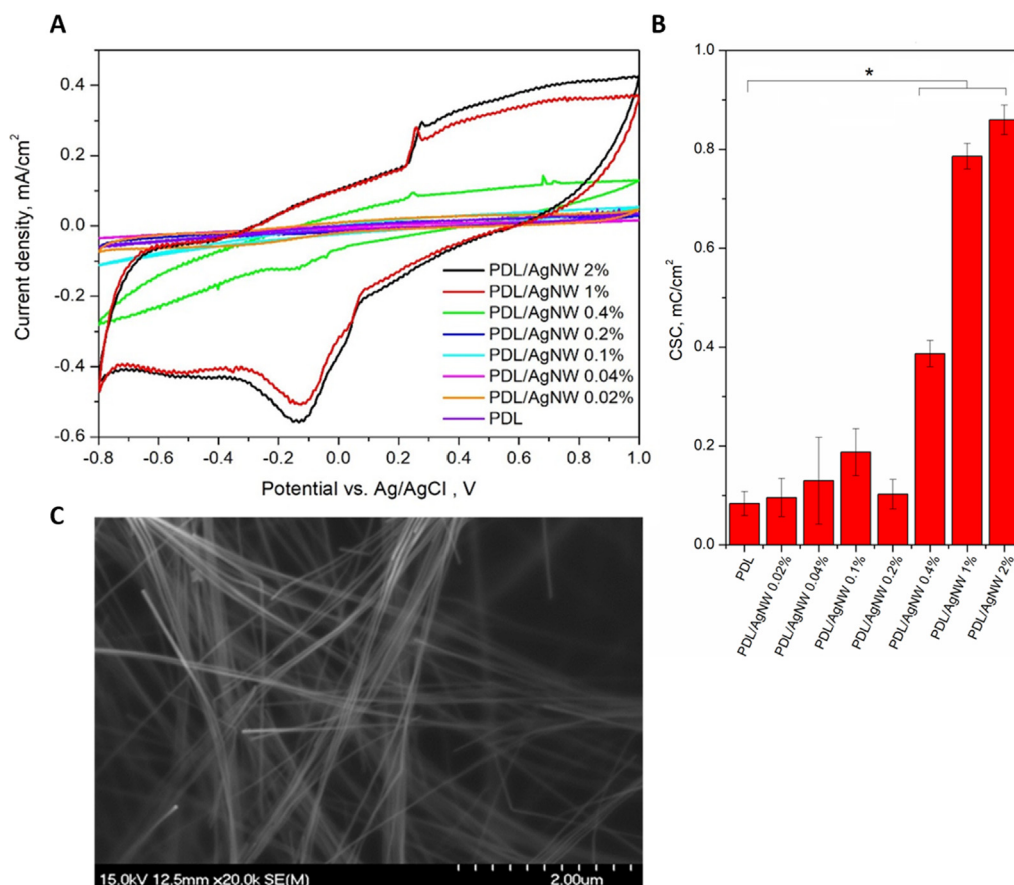
Fig. 1. Determination of the electrochemical percolation threshold in PDL/AgNW nanocomposites. Cyclic voltammetric curves of nanocomposites with different ratios of PDL-to-AgNWs (A) and corresponding charge storage capacities (B). SEM micrograph of PDL/AgNW 2% w/w composite showing the extended percolation network of AgNWs (C). Results are presented as the mean ± STD, ★ = p < 0.05, n = 3.

percolation threshold for the AgNWs in a PDL matrix was observed to occur at a surface density of ~65 mg/m^2, corresponding to a AgNWs loading of 0.4% w/w.
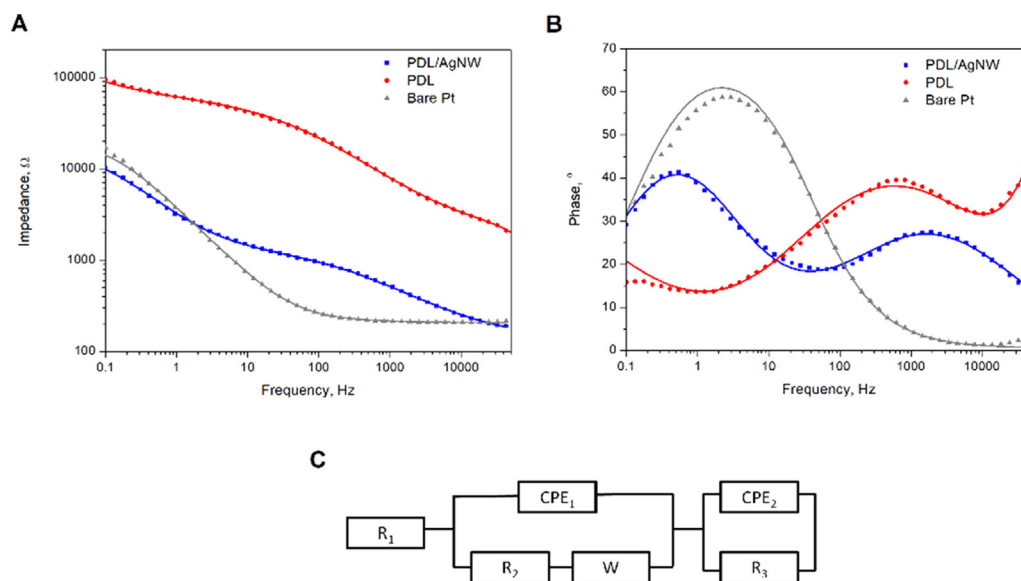
3.2. Electrochemical characterization

Electrochemical impedance analysis expressed as a Bode plot (Fig. 2A) indicated that the impedance modulus as a function of frequency was the lowest for Pt electrodes (for frequencies above 1 Hz) and PDL/AgNW (for frequencies below 1 Hz). Conversely, pristine PDL exhibited a strongly resistive behaviour with an impedance profile approaching 100 kΩ at 0.1 Hz. The analysis of the phase angle profile (Fig. 2B) of Pt and pristine PDL shows that these two materials exhibited one major capacitive peak at 2 Hz and 700 Hz, respectively. In contrast, the phase profile of PDL/AgNW nanocomposites demonstrated two capacitive peaks at 0.5 Hz and 2000 Hz.

To model the behaviour of PDL- and PDL/AgNW-coated Pt electrodes, a modified Randles circuit was used. As shown in Fig. 2C, R1 represents the solution resistance, R_2 is the charge transfer resistance incurred during the electrochemical reactions taking place on the electrodes. CPE_1 is the constant phase element modelling the non-faradaic processes, W is the Warburg element representing the diffusion control process, R_3 is the resistance to charge conduction in the PDL/AgNW interphase layer and CPE_2 describes the charge capacitance of the solid electrolyte interphase layer [31]. The quality of fitting is demonstrated by the fitted curves (Fig. 2B) and low deviation between experimental and fitted data (2.3% and 3.4% for PDL/AgNW and PDL, respectively).

High conductivity and a strong capacitive behaviour are essential requirements for the development of novel conductive inks in wearable electronics, soft robotics and implantable biomedical devices. The shift in the phase-angle peak position, noted for Pt and PDL, indicated differences in the capacitive behaviour of these two materials, governed by the double-layer effects for pristine PDL and faradaic reactions for Pt [32]. Conversely, two capacitive peaks noted in the phase profile of PDL/AgNW nanocomposites arise from the faradaic reaction of AgNWs (Ag ↔ Ag$^+$) and the double-layer capacitance of PDL, respectively. Similar capacitive behavior was observed when AgNWs were used as a filler for poly(ε-decalactone) [33].

Although these EIS results show the overall impedance of the electrode system, the electrical behavior of the system was further evaluated with the use of an equivalent circuit model. The results of EIS fitting confirmed that the PDL component itself is a poor conductor, with a resistivity of 52.9 ± 1.6 kΩ·cm^2. The addition of AgNWs significantly improved the conductivity of the polymer, resulting in a resistance of 1.13 ± 0.03 kΩ (sheet resistance of approx. 320 ± 9 Ω/sq). Simultaneously, the presence of AgNWs improved the capacitance of PDL, achieving a value of 0.583 ± 0.0 16 μF (2.06 ± 0.06 μF/cm^2) for PDL nanocomposites formulated with 2% w/w AgNW, five times higher than for pristine PDL (0.10 5 ± 0.003 μF). Critically, this PDL/AgNW nanocomposite was shown to outperform previously described conducting bioinks, specifically, PEDOT (resistance ~16 kΩ, capacitance ~0.17 μF) [34], a composite of polyethylene glycol diacrylate and silver nanoparticles (resistance ~500 kΩ) [35], or a bioactive hydrogel of PEDOT:PSS in poly(2-hydroxyethyl methacrylate-co-polyethyleneglycol

Fig. 2. Electrochemical characterisation of PDL and PDL/AgNW. EIS analysis in the form of Bode plots of impedance modulus vs. frequency (A) and phase angle vs. frequency (B) for PDL and PDL/AgNW, as well as a Pt coated glass electrode; dots represent experimental data, while lines represent simulated results. Equivalent circuit model used for the fitting of the data collected for PDL and PDL/AgNW (C).

methacrylate) matrix (resistance ~100 kΩ) urthermore, 2% w/w PDL/AgNW nanocomposites were found to exhibit a lower sheet resistance when compared to other conducting materials used in the design of pressure sensor devices, including single walled carbon nanotubes/alginate hydrogel spheres (sheet resistance of 25 kΩ/sq) [36] and paper/carbon nanotube composites (12.6 kΩ/sq) [37].

3.3. Mechanical analysis of pristine and PDL/AgNW composites

Rheological testing of pristine PDL and PDL/AgNW nanocomposites inks was performed to determine the materials viscoelastic properties (Fig. 3A). PDL dissolved in THF at 37 °C acted as a viscous liquid with notably high surface tension. To form the conductive polymer blend, AgNWs dispersed in ethanol were combined with PDL at a concentration of 2% w/w. The storage modulus of both pristine PDL and 2% w/w AgNW PDL nanocomposites after curing was assessed over a range of shear strains under constant angular frequency of 1 Hz and is presented in Fig. 3B. The viscosity of pristine PDL liquids increased incrementally with PDL concentration whereas it was noted that PDL/AgNW composites show a Newtonian behavior at low shear strains followed by a pseudoplastic behavior, commonly seen in non-Newtonian polymer liquids above a critical strain rate (ε_{cr}) of 35–40%[38]. From these findings, no notable difference in the critical strain rate between inks formulated with 2% w/w AgNWs, relative to inks formulated with pristine PDL, indicating that AgNWs do not lead to an increase in PDL chain disentanglement. PDL/AgNW bioinks formulated with 0.3% w/v polymer concentrations possessed the highest viscosity of all bioink formulations. It can be hypothesized that owing to the viscoelastic properties of this PDL/AgNW bioink, this formulation would perform well in extrusion based additive manufacturing where viscous deformation would be minimized following ink extrusion, ensuring high-fidelity printing.

As observed in Fig. 3b, the 2% w/w PDL/AgNW nanocomposite materials possessed an increased storage modulus relative to pristine PDL, a common phenomenon in polymer composites formulated with metal particulates. As the biosensor was formed predominantly from pristine PDL, with an aim to recording pathological swelling of the brain, it was important that the mechanical

properties of this polymer mimic that of tissues of the central nervous system. It has been be reported that the dura mater possesses an elastic modulus of 30–100 MPa, significantly higher than that of PDL, which we measured to be 220 kPa, providing reassurance that the PDL biosensor device would not induce an inflammatory response as a result of mechanical mismatch induced shear stresses [39].

3.4. Design & fabrication of a PDL/AgNW composite strain biosensor via additive manufacturing

Different electrode geometries were designed with Autodesk inventor Computer Aided software. Initially, a simple linear electrode design was used to optimise the 3D printing process. Following this, electrodes of increasing complexity were designed and processed using GeSIM slicing software (Supplementary Fig S1). A final design of 60 interdigitated electrodes was used in the strain sensing experiments as the proximity of the 3D-printed conductive ink probes facilitated high sensitivity acquisition of changes in resistance due to mechanical strain.

A 2% w/w PDL/AgNW composite was dissolved in THF in order to produce an extrudable viscous slurry which was loaded into a 5 ml syringe with a 150 μm lured needle. Extrusion printing parameters were determined as a 5 mms^{-1} print speed, 75 kPa extrusion pressure and a syringe temperature of 37 °C. The conductive ink was extruded onto thermanox (Fig. 4A) and pristine PDL films (Fig. 4B, C) as shown in the supplementary information (Movie S1). Light microscopy indicated a high fidelity of electrode printing (Fig. 4D) and a high density of nanowires present in the composite (Fig. 4E).

3.5. In vitro biocompatibility

Immunofluorescent analysis (Fig. 5A–C) was performed to quantify the cell density of astrocytes and neurons (Fig. 5D) and the mean area of the astrocyte cell soma (Fig. 5E) in mixed neural populations cultured on bare Pt, PDL and PDL/AgNW substrates. The lowest percentage of astrocytes was noted for PDL/AgNW (11.3% ± 0.4%), considerably lower than control Pt (28.2% ± 5.0%) and PDL substrates (27.3% ± 9.4%). Analysis of the mean astrocyte

A

B
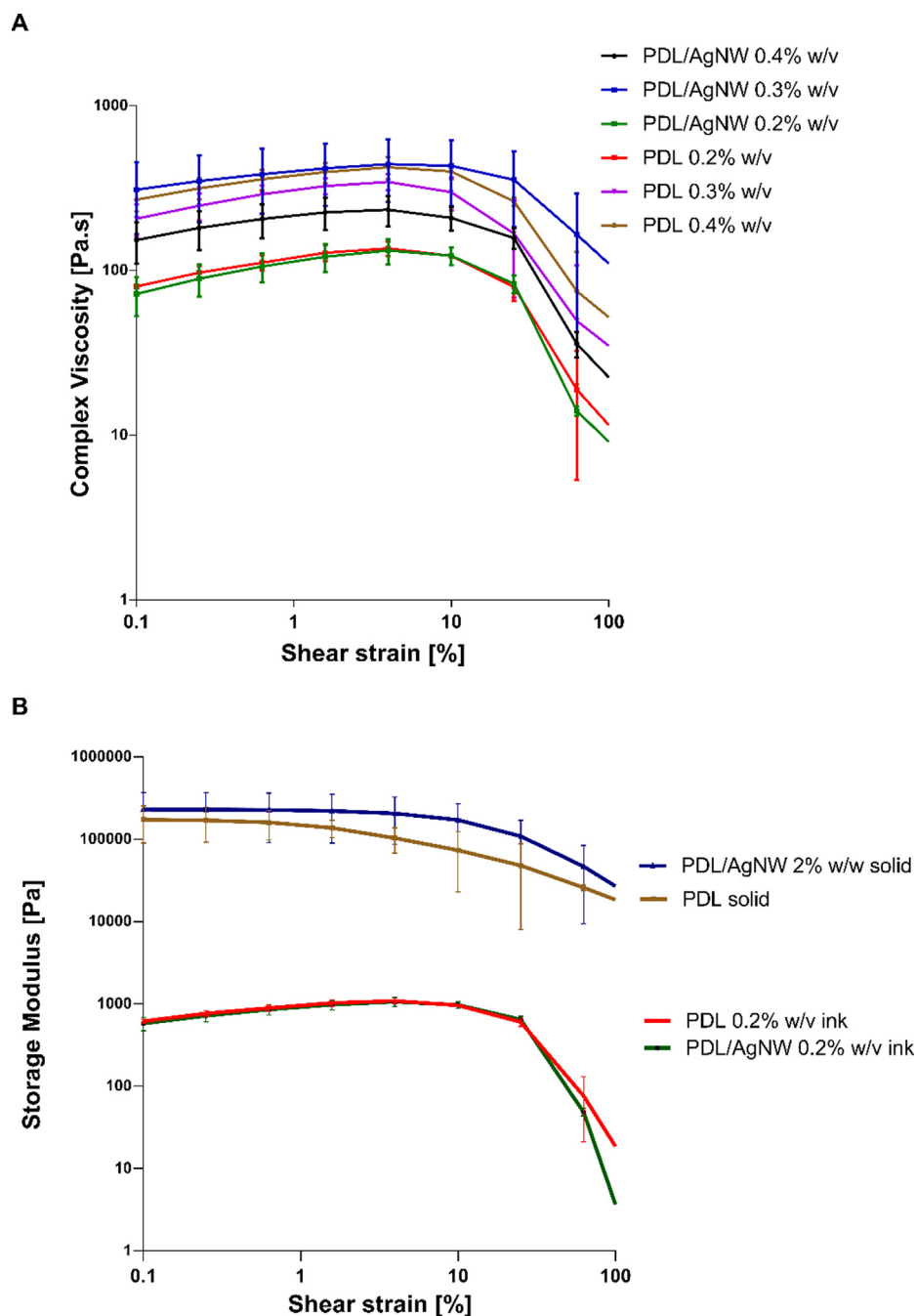
Fig. 3. Rheological behavior of pristine PDL and PDL/AgNW inks and materials. The viscoelastic properties of PDL & PDL/AgNW composites (A), The storage modulus of the of inks and solid polymers was assessed as a function of shear strain (B).

cell area indicated that astrocytes cultured on PDL/AgNW nanocomposite materials possessed a mean cell area of 716 ± 99 μm², significantly less that than astrocytes cultured on control Pt (1105 ± 161 μm²) as well as control pristine PDL substrates (893 ± 130 μm²).

From our cytocompatibility analysis using VM cells, it was observed that pristine and PDL/AgNW nanocomposite materials supported cell adhesion and neuron viability, Interestingly, PDL/AgNW nanocomposite were associated with significant decreases in astrocyte number and area, cells which typically become activated in response to a foreign body [40], increasing in size and abundance indicating that PDL/AgNW nanocomposites demonstrated increased biocompatibility relative to control Pt and pristine PDL. PDL/AgNW *in vitro*. Critically, reduced astrocyte

activation has been shown to reduce fibrosis and implant encapsulation in vivo, an important contribitor to device failure [22,41,42].

3.6. In-vitro stress/strain sensing

The biosensor functionality of optimized PDL/AgNW nanocomposite formulations was characterised *in vitro* using an apparatus that mechanically actuated the biosensor at a cyclic loading rate of 0.5 Hz. The relative change in impedance was measured while a cyclic strain of 5% was applied to the sensor and changes in impedance was measured at a frequency of 1 kHz. We choose a strain of 5% based on the results from rheological analysis of PDL/AgNW nanocomposites (Fig. 3). It can be seen that the strain of 5% corresponds to a stress in the order of 1 kPa strain which was chosen to
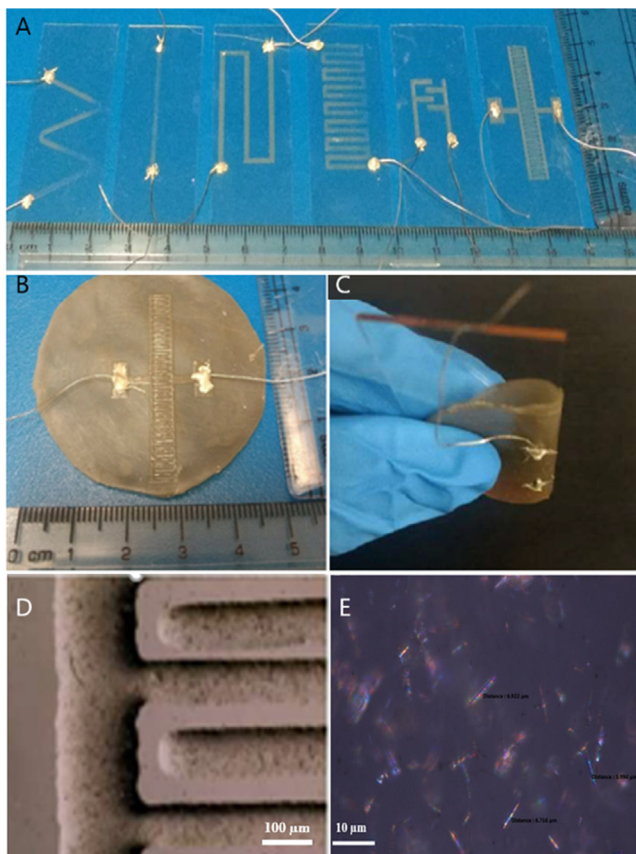
Fig. 4. Extrusion printing of conductive AgNW/PDL nanocomposite inks. AgNW/PDL inks were extruded onto thermanox (A) and pristine cast PDL substrates (B). The flexibility of the extrusion printed biosensors is illustrated in (C). Brightfield microscopic image of extrusion printed biosensor electrodes (D) and a digital microscopic image of silver nanowires embedded into the PDL matrix (E).

emulate pathological stresses described in the literature [3,7]. The relative change in impedance due to mechanical load was expressed as the strain gauge factor: $\Delta Z/Z_0$, were ΔZ is the change in impedance, and Z_0 is the impedance under static conditions. The sensitivity of the biosensors was assessed over the course of 21 days under cyclic mechanical strain to determine the resilience of the PDL/AgNW polymer composite to simulated physiological conditions (Fig. 6).

In this experiemnt, we have shown that sensor designs of micron scale resolution can be printed onto flexible substrates, and can be used to monitor cyclic strain forces for up to 21 days *in vitro* or approximately one million strain cycles. It was observed that PDL/AgNW nanocomposite strain sensors were sensitive to pathologically relevant stresses which have been measured to range from approx. 7–50 mm Hg (1–7 kPa) in studies on brain swelling [43,44].

Towards the end of the cyclic strain testing, the impedance response of the device was observed to fluctuate. This phenomenon can be attributed to the combined hysteresis loss and damage model of reinforced elastomers, derived from the breakage and formation of particle agglomerates under strain conditions. Specifically, it has been shown that diverse electron tunnelling effects when nanocomposite materials are subjected to cyclic strain conditions and that conducting particles in close proximity produce an increased tunnelling effect under relaxed condition. Here, the observed continuous reduction in resistance behaviour can be attributed to the formation of new physical bonds between conducting particles and the elastomer matrix when subjected to

strain/relaxation cycles, similar to the loss energy factor and hysteresis loss also observed in elastomeric composites. This continuous change in impedance can be improved through optimisation of the processing window and by employing a processing technique described by us previously [45]. Critically, previous studies have reported a similar loss in sensitivity (gauge factor) at 1% strain after ca. 12,600 strain cycles in a similar elastomeric composite [8].

Similar work by Rogers et al. has focused on the development of an intracranial pressure sensor device that remained functional for 3 days, and which they report was sufficient for acute intracranial pressure monitoring [3]. In this study, they report on the standards defined by the Association for the Advancement of Medical Instrumentation (AAMI) for pressure monitoring, that is, accuracy loss for pressure sensors should not exceed ± 10% for devices intended to measure in the 2.67 to 13.33 kPa (20–100 mm Hg) range [46]. In our study, a 75 mm Hg (10 kPa) stress was exerted on the sensor when exposed to 5% uniaxial stain, with a standard error of mean of 9.66%. From our biosensor functionality experiments, we noted an average strain gauge factor over all strain cycles of 2.78 ± 0.22. These finding indicated that PDL-AgNW sensors developed in this study fall within the standards of the AAMI for functionality and may facilitate longer clinical monitoring of pressure in vivo.

## 4. Summary and conclusion

In this study, we describe the development of a PDL biosensor that can measure changes in physiologically relevant mechanical forces for three weeks *in vitro*. We have shown that an environmentally friendly polymer produced using fungal biotechnology can be used to develop flexible electronic inks. We demonstrated that modern additive manufacturing technologies can be used to fabricate microscale interdigitated electrode designs using a direct write process. In order to generate inks with high electrical conductivity, we established a silver nanowire percolation network within a PDL matrix, achieving a low electrical resistance (320 ± 9 Ω/sq) and a high electrical capacitance (2.06 ± 0.06 μF/cm^2) with a low nanowire content (1% w/w). The rheological testing results revealed that bioinks achieved a low and constant viscosity (90–500 kPa.s) at shear strain rates between 1 and 35%, typical for Newtonian viscous polymer liquids. Furthermore, the elastic modulus of cured PDL (220 kPa) was found to be significantly lower than that of the dura mater (30–100 MPa), providing reassurance that the PDL biosensor device would not induce an inflammatory response as a result of mechanical mismatch induced shear stresses. Furthermore, we demonstrated that PDL nanocomposite inks could support the attachment and survival of a mixed neural cell population for a ten-day period *in vitro*.

We have shown that electrodes of micron scale resolution can be printed onto flexible substrates, and as-formed sensors can be used to monitor cyclic strain forces for up to 21 days *in vitro* or approximately one million strain cycles. We propose that these soft, flexible and biocompatible biosensors may be integrated into a range of medical devices to detect real-time changes in tissue dynamics and elicit a compensatory response from the device, to transition into an era of self-regulating medical implants.

Authors' contributions

MJPB, JRS, JB and KK conceived off the research project while JB, KK, MB, UF and MC contributed to the processing of data and preparation of this manuscript.

JB performed rheological analysis of the polymer composites and designed the biosensors using Autodesk inventor CAD software. JB optimised the GeSIM bioscaffolder process and the testing of sensor sensitivity to uniaxial strain using potentiometry. JB
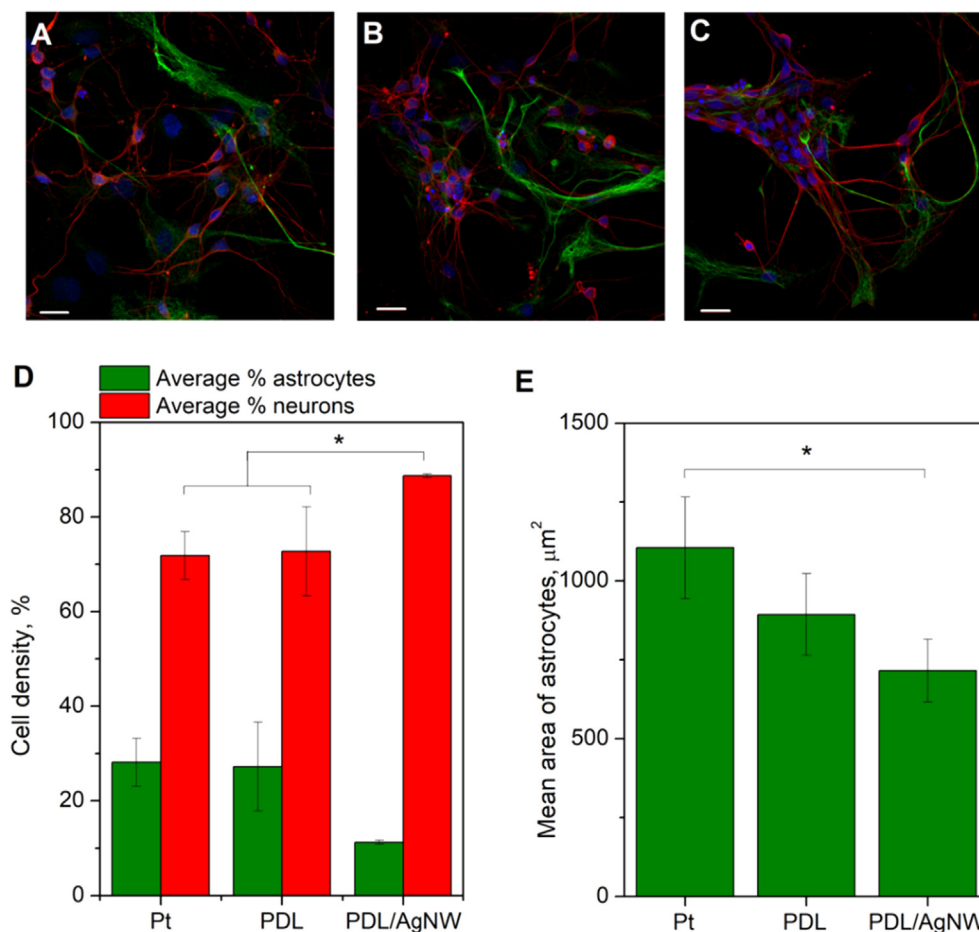
Fig. 5. Cytocompatability analysis of PDL and a PDL/AgNW nanocomposite. Representative fluorescent images of primary ventral mesencephalic (VM) mixed cell population cultured for 7 days on Pt (A), PDL (B) and PDL/AgNW nanocomposite materials (C); neurons are visualised by anti-β-tubulin III (red), astrocyte cells by anti-glial fibrillar acidic protein, GFAP stain (green) and nuclei by 4′,6-diamidino-2-phenylindole, DAPI (blue); the scale bar is 20 μm. Cell density analysis of astrocyte and neurons (D) and the mean area of the astrocyte cell body (E) on Pt, PDL and PDL/AgNW nanocomposites after 7 days of culture; results are presented as the mean ± STD, ★ = $p < 0.05$, n = 3 (biological replicates). (For interpretation of the references to colour in this figure legend, the reader is referred to the web version of this article.)

captured the brightfield and digital microscopic Images. JB interpreted the acquired data and described the results.

KK optimised PDL/AgNW formulations, carried out SEM measurements, electrochemical measurements, and biological studies, interpreted the acquired data and described the results.

MC was a Biomedical Engineering master's student under the supervision of MB and under the direct lab supervision of JB. MC was instrumental to the optimisation of the extrusion-based 3D printing and the testing of biosensors using potentiometry.

AP contributed intellectually to this project with extensive knowledge in polymer processing and sensor development.

JF was responsible for the synthesis and characterisation of PDL under the supervision of JRS. All authors have read and approved the manuscript.

Declaration of Competing Interest

The authors declare that they have no known competing financial interests or personal relationships that could have appeared to influence the work reported in this paper.

Acknowledgements

Appendix A. Supplementary material

Supplementary data to this article can be found online at https://doi.org/10.1016/j.matdes.2021.109700.

References

[1] H.C. Koydemir, A. Ozcan, Wearable and implantable sensors for biomedical applications, Ann. Rev. Analyt. Chem. 11 (1) (2018) 127–146, https://doi.org/10.1146/annurev-anchem-061417-125956.
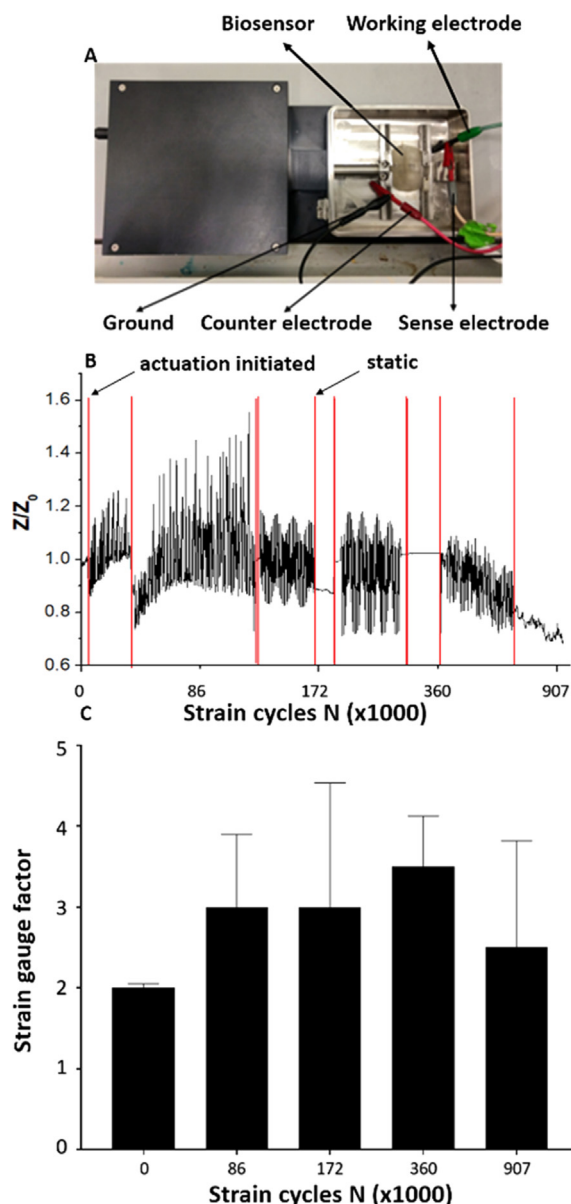
Fig. 6. In vitro analysis of biosensor functionality under cyclic loading conditions. (A) Image of the Cellscale bioreactor used to assess the sensitivity of the PDL/AgNW device under dynamic conditions while maintained in PBS at 37 °C. (B) The sensitivity of the biosensor as a function of cyclic strain (red lines indicate when the actuation system was switched on/off. (C) Long-term stability of the biosensor after 907,000 strain cycles. (For interpretation of the references to colour in this figure legend, the reader is referred to the web version of this article.)

[2] M. Mathew, S. Radhakrishnan, A. Vaidyanathan, B. Chakraborty, C.S. Rout, Flexible and wearable electrochemical biosensors based on two-dimensional materials: Recent developments, Anal. Bioanal. Chem. 413 (3) (2021) 727–762, https://doi.org/10.1007/s00216-020-03002-y.

[3] S.-K. Kang, R.K.J. Murphy, S.-W. Hwang, S.M. Lee, D.V. Harburg, N.A. Krueger, J. Shin, P. Gamble, H. Cheng, S. Yu, Z. Liu, J.G. McCall, M. Stephen, H. Ying, J. Kim, G. Park, R.C. Webb, C.H. Lee, S. Chung, D.S. Wie, A.D. Gujar, B. Vemulapalli, A.H. Kim, K.-M. Lee, J. Cheng, Y. Huang, S.H. Lee, P.V. Braun, W.Z. Ray, J.A. Rogers, Bioresorbable silicon electronic sensors for the brain, Nature 530 (2016) 71–76, https://doi.org/10.1038/nature16492.

[4] Q. Meng, Z. Liu, S. Han, L. Xu, S. Araby, R. Cai, Y. Zhao, S. Lu, T. Liu, A facile approach to fabricate highly sensitive, flexible strain sensor based on elastomeric/graphene platelet composite film, J. Mater. Sci. 54 (15) (2019) 10856–10870, https://doi.org/10.1007/s10853-019-03650-1.

[5] C. Pang, G.-Y. Lee, T.-I. Kim, S.M. Kim, H.N. Kim, S.-H. Ahn, K.-Y. Suh, A flexible and highly sensitive strain-gauge sensor using reversible interlocking of nanofibres, Nat. Mater. 11 (9) (2012) 795–801, https://doi.org/10.1038/nmat3380.

[6] N. Canac, K. Jalaleddini, S.G. Thorpe, C.M. Thibeault, R.B. Hamilton, Review: pathophysiology of intracranial hypertension and noninvasive intracranial

[7] Q. Yang, S. Lee, Y. Xue, Y. Yan, T.-L. Liu, S.-K. Kang, Y.J. Lee, S.H. Lee, M.-H. Seo, D. Lu, J. Koo, M.R. MacEwan, R.T. Yin, W.Z. Ray, Y. Huang, J.A. Rogers, Materials, mechanics designs, and bioresorbable multisensor platforms for pressure monitoring in the intracranial space, Adv. Funct. Mater. 30 (17) (2020) 1910718, https://doi.org/10.1002/adfm.201910718.

[8] G. Tadayyon, K. Krukiewicz, J. Britton, A. Larrañaga, C. Vallejo-Giraldo, M. Fernandez-Yague, Y. Guo, G. Orpella-Aceret, L. Li, A. Poudel, M.J.P. Biggs, In vitro analysis of a physiological strain sensor formulated from a PEDOT:PSS functionalized carbon nanotube-poly(glycerol sebacate urethane) composite, Mater. Sci. Eng., C 121 (2021) 111857, https://doi.org/10.1016/j.msec.2020.111857.

[9] N.D. Sanandiya, Y. Vijay, M. Dimopoulou, S. Dritsas, J.G. Fernandez, Large-scale additive manufacturing with bioinspired cellulosic materials, Sci. Rep. 8 (1) (2018) 8642, https://doi.org/10.1038/s41598-018-26985-2.

[10] Y. Zhu, C. Romain, C.K. Williams, Sustainable polymers from renewable resources, Nature 540 (7633) (2016) 354–362, https://doi.org/10.1038/nature21001.

[11] J.A. Wilson, S.A. Hopkins, P.M. Wright, A.P. Dove, Synthesis of ω-pentadecalactone copolymers with independently tunable thermal and degradation behavior, Macromolecules 48 (4) (2015) 950–958, https://doi.org/10.1021/ma5022049.

[12] A. Youssef, S.J. Hollister, P.D. Dalton, Additive manufacturing of polymer melts for implantable medical devices and scaffolds, Biofabrication 9 (1) (2017) 012002, https://doi.org/10.1088/1758-5090/aa5766.

[13] S.Y. Chin, Y.C. Poh, A.-C. Kohler, J.T. Compton, L.L. Hsu, K.M. Lau, S. Kim, B.W. Lee, F.Y. Lee, S.K. Sia, Additive manufacturing of hydrogel-based materials for next-generation implantable medical devices, Sci. Robot. 2 (2) (2017) eaah6451, https://doi.org/10.1126/scirobotics.aah6451.

[14] C. O'Mahony, E.U. Haq, C. Sillien, S.A.M. Tofail, Rheological issues in carbon-based inks for additive manufacturing, Micromachines 10 (2) (2019), https://doi.org/10.3390/mi10020099.

[15] B. Elder, R. Neupane, E. Tokita, U. Ghosh, S. Hales, Y.L. Kong, Nanomaterial patterning in 3D printing, Adv. Mater. (Deerfield Beach, Fla.) 32 (17) (2020), https://doi.org/10.1002/adma.201907142.

[16] Y. Ahn, H. Lee, D. Lee, Y. Lee, Highly conductive and flexible silver nanowire-based microelectrodes on biocompatible hydrogel, ACS Appl. Mater. Interfaces 6 (21) (2014) 18401–18407, https://doi.org/10.1021/am504462f.

[17] S.G. Lehmann, D. Toybou, A.-E. Pradas del Real, D. Arndt, A. Tagmount, M. Viau, M. Safi, A. Pacureanu, P. Cloetens, S. Bohic, M. Salomé, H. Castillo-Michel, B. Omaña-Sanz, A. Hofmann, C. Vulpe, J.-P. Simonato, C. Celle, L. Charlet, B. Gilbert, Crumpling of silver nanowires by endolysosomes strongly reduces toxicity, Proc. Natl. Acad. Sci. 116 (30) (2019) 14893, https://doi.org/10.1073/pnas.1820041116.

[18] G.-J. Zhu, P.-G. Ren, J. Wang, Q. Duan, F. Ren, W.-M. Xia, D.-X. Yan, A Highly sensitive and broad-range pressure sensor based on polyurethane mesodome arrays embedded with silver nanowires, ACS Appl. Mater. Interfaces 12 (17) (2020) 19988–19999, https://doi.org/10.1021/acsami.0c03697.

[19] J. Fernández, A. Etxeberria, A.L. Varga, J.-R. Sarasua, Synthesis and characterization of ω-pentadecalactone-co-ε-decalactone copolymers: evaluation of thermal, mechanical and biodegradation properties, Polymer 81 (2015) 12–22, https://doi.org/10.1016/j.polymer.2015.11.001.

[20] A.S. Bondarenko, G.A. Ragoisha, Progress in Chemometrics Research, Nova Science Publishers, 2005.

[21] I.R. Minev, P. Musienko, A. Hirsch, Q. Barraud, N. Wenger, E.M. Moraud, J. Gandar, M. Capogrosso, T. Milekovic, L. Asboth, R.F. Torres, N. Vachicouras, Q. Liu, N. Pavlova, S. Duis, A. Larmagnac, J. Vörös, S. Micera, Z. Suo, G. Courtine, S.P. Lacour, Electronic dura mater for long-term multimodal neural interfaces, Science 347 (6218) (2015) 159, https://doi.org/10.1126/science.1260318.

[22] C. Vallejo-Giraldo, K. Krukiewicz, I. Calaresu, J. Zhu, M. Palma, M. Fernandez-Yague, B.W. McDowell, N. Peixoto, N. Farid, G. O'Connor, L. Ballerini, A. Pandit, M.J.P. Biggs, Attenuated glial reactivity on topographically functionalized poly (3,4-Ethylenedioxythiophene):P-toluene sulfonate (PEDOT:PTS) neuroelectrodes fabricated by microimprint lithography, Small 14 (2018), https://doi.org/10.1002/smll.201800863.

[23] C. Vallejo-Giraldo, E. Pugliese, A. Larranaga, M.A. Fernandez-Yague, J.J. Britton, A. Trotier, G. Tadayyon, A. Kelly, I. Rago, J.R. Sarasua, E. Dowd, L.R. Quinlan, A. Pandit, M.J. Biggs, Polyhydroxyalkanoate/carbon nanotube nanocomposites: flexible electrically conducting elastomers for neural applications, Nanomedicine (London, England) 11 (19) (2016) 2547–2563, https://doi.org/10.2217/nnm-2016-0075.

[24] C. Vallejo-Giraldo, N.P. Pampaloni, A.R. Pallipurath, P. Mokarian-Tabari, J. O'Connell, J.D. Holmes, A. Trotier, K. Krukiewicz, G. Orpella-Aceret, E. Pugliese, L. Ballerini, M. Kilcoyne, E. Dowd, L.R. Quinlan, A. Pandit, P. Kavanagh, M.J.P. Biggs, Preparation of cytocompatible ITO neuroelectrodes with enhanced electrochemical characteristics using a facile anodic oxidation process, Adv. Funct. Mater. 28 (12) (2018) 1605035, https://doi.org/10.1002/adfm.201605035.

[25] D.I. Friedman, G.T. Liu, K.B. Digre, Revised diagnostic criteria for the pseudotumor cerebri syndrome in adults and children, Neurology 81 (13) (2013) 1159–1165, https://doi.org/10.1212/WNL.0b013e3182a55f17.

[26] D.R. Merrill, Chapter 6 – The Electrode – Materials and Configurations, in: J.E. Arle, J.L. Shils (Eds.), Essential Neuromodulation, Academic Press, San Diego, 2011, pp. 107–152.

[27] L. Qi, B.I. Lee, S. Chen, W.D. Samuels, G.J. Exarhos, High-dielectric-constant silver-epoxy composites as embedded dielectrics, Adv. Mater. 17 (14) (2005) 1777–1781, https://doi.org/10.1002/adma.200401816.

[28] I. Barandiaran, J. Gutierrez, A. Tercjak, G. Kortaberria, Thin film nanocomposites based on SBM triblock copolymer and silver nanoparticles: morphological and dielectric, Analysis 302 (10) (2017) 1700169, https://doi.org/10.1002/mame.201700169.

[29] J. Wang, J. Jiu, M. Nogi, T. Sugahara, S. Nagao, H. Koga, P. He, K. Suganuma, A highly sensitive and flexible pressure sensor with electrodes and elastomeric interlayer containing silver nanowires, Nanoscale 7 (7) (2015) 2926–2932, https://doi.org/10.1039/C4NR06494A.

[30] D.P. Langley, G. Giusti, M. Lagrange, R. Collins, C. Jiménez, Y. Bréchet, D. Bellet, Silver nanowire networks: physical properties and potential integration in solar cells, Sol. Energy Mater. Sol. Cells 125 (2014) 318–324, https://doi.org/10.1016/j.solmat.2013.09.015.

[31] K. Yao, J.P. Zheng, Z. Liang, Binder-free freestanding flexible Si nanoparticle–multi-walled carbon nanotube composite paper anodes for high energy Li-ion batteries, J. Mater. Res. 33 (4) (2018) 482–494, https://doi.org/10.1557/jmr.2017.475.

[32] M. Mahdavian, M.M. Attar, Another approach in analysis of paint coatings with EIS measurement: phase angle at high frequencies, Corros. Sci. 48 (12) (2006) 4152–4157, https://doi.org/10.1016/j.corsci.2006.03.012.

[33] K. Krukiewicz, J. Fernandez, M. Skorupa, D. Więcławska, A. Poudel, J.-R. Sarasua, L.R. Quinlan, M.J.P. Biggs, Analysis of a poly(ε-decalactone)/silver nanowire composite as an electrically conducting neural interface biomaterial, BMC Biomed. Eng. 1 (1) (2019) 9, https://doi.org/10.1186/s42490-019-0010-3.

[34] J. Yang, D.C. Martin, Microporous conducting polymers on neural microelectrode arrays: II. Physical characterization, Sens. Actuators A: Phys. 113 (2) (2004) 204–211, https://doi.org/10.1016/j.sna.2004.02.029.

[35] E. Fantino, A. Chiappone, I. Roppolo, D. Manfredi, R. Bongiovanni, C.F. Pirri, F. Calignano, 3D printing: 3D printing of conductive complex structures with in situ generation of silver nanoparticles (Adv. Mater. 19/2016), Adv. Mater. (Deerfield Beach, Fla.) 28 (19) (2016) 3711, https://doi.org/10.1002/adma.201670132.

[36] Y. Tai, M. Mulle, I. Aguilar Ventura, G. Lubineau, A highly sensitive, low-cost, wearable pressure sensor based on conductive hydrogel spheres, Nanoscale 7 (35) (2015) 14766–14773, https://doi.org/10.1039/C5NR03155A.

[37] Z. Zhan, R. Lin, V.-T. Tran, J. An, Y. Wei, H. Du, T. Tran, W. Lu, Paper/carbon nanotube-based wearable pressure sensor for physiological signal acquisition and soft robotic skin, ACS Appl. Mater. Interfaces 9 (43) (2017) 37921–37928, https://doi.org/10.1021/acsami.7b10820.

[38] J.M. Ugartemendia, M.E. Muñoz, A. Santamaria, J.R. Sarasua, Supramolecular structure, phase behavior and thermo-rheological properties of a poly (l-lactide-co-ε-caprolactone) statistical copolymer, J. Mech. Behav. Biomed. Mater. 48 (2015) 153–163, https://doi.org/10.1016/j.jmbbm.2015.04.007.

[39] J. Zwirner, M. Scholze, J.N. Waddell, B. Ondruschka, N. Hammer, Mechanical properties of human dura mater in tension - an analysis at an age range of 2 to 94 years, Sci. Rep. 9 (1) (2019) 16655, https://doi.org/10.1038/s41598-019-52836-9.

[40] A. Goudriaan, N. Camargo, K. Carney, S. Oliet, A. Smit, M. Verheijen, Novel cell separation method for molecular analysis of neuron-astrocyte co-cultures, Front. Cell. Neurosci. 8 (2014) 12, https://doi.org/10.3389/fncel.2014.00012.

[41] M.T. Noori, S.C. Jain, M.M. Ghangrekar, C.K. Mukherjee, Biofouling inhibition and enhancing performance of microbial fuel cell using silver nano-particles as fungicide and cathode catalyst, Bioresour. Technol. 220 (2016) 183–189, https://doi.org/10.1016/j.biortech.2016.08.061.

[42] M. Gulino, D. Kim, S. Pané, S.D. Santos, A.P. Pêgo, Tissue response to neural implants: the use of model systems toward new design solutions of implantable microelectrodes, Front. Neurosci. 13 (2019) 689, https://doi.org/10.3389/fnins.2019.00689.

[43] U. Kawoos, M. Gu, J. Lankasky, R.M. McCarron, M. Chavko, Effects of exposure to blast overpressure on intracranial pressure and blood-brain barrier permeability in a rat model, PLoS ONE 11 (12) (2016) e0167510, https://doi.org/10.1371/journal.pone.0167510.

[44] S. Angeli, T. Stylianopoulos, Experimental measurements and mathematical modeling towards quantification of brain swelling stress, J. Biomech. 56 (2017) 42–47, https://doi.org/10.1016/j.jbiomech.2017.02.028.

[45] A. Poudel, N. Karode, P. McGorry, P. Walsh, J.G. Lyons, J. Kennedy, S. Matthews, A. Coffey, Processing of nanocomposites using supercritical fluid assisted extrusion for stress/strain sensing applications, Compos. B Eng. 165 (2019) 397–405, https://doi.org/10.1016/j.compositesb.2019.01.098.

[46] VI. Indications for Intracranial Pressure Monitoring, 24(supplement 1) (2007) S-37-S-44. https://doi.org/10.1089/neu.2007.9990.